Theoretical modelling the electronic structure and magnetic properties of LiFeAs and FeSe

Wei Wu[1,2*]
Department of Materials and London Centre for Nanotechnology, Imperial College London, South Kensington Campus, London, SW7 2AZ, U.K.[1] *and UCL Department of Physics and Astronomy and London Centre for Nanotechnology, University College London, Gower Street, London, WC1E 6BT, U.K.*[2]

The electronic structure and magnetic properties of iron-base superconductors including lithium-iron-arsenic (LiFeAs) and iron-selenium (FeSe) have been studied using density functional theory and hybrid functional. The computed anti-ferromagnetic exchange interactions for the first (second) nearest neighbouring iron atoms in LiFeAs and FeSe are approximately 16 (81) meV and 6 (13) meV respectively. These results are in agreement with previous theoretical calculations and experiments. The total energies for LiFeAs and FeSe unit cell of different spin configurations on iron atoms including non-magnetic, spin-1, and spin-2 are also calculated. The lowest state has a spin-2 configuration for LiFeAs and FeSe. These calculations show the co-existence of the complicated band structure around the valence band and conduction band and *d*-orbital magnetism. The theoretical results presented here are particularly useful for the experimentalists working on the electronic structure and magnetism of LiFeAs and FeSe.

PACS numbers: 31.15.E-,71.70.Gm,75.30.Et,74.70.Xa,74.20.-z,74.20.Pq

I. INTRODUCTION

Cuprate-based superconductors (CuSCs) have the highest superconducting transition temperature achieved to date in HgBaCaCuO ($T_c \sim 200$ K) [1]. By contrast a rather new class of high-T_c superconductors (HTSC), iron-based superconductors (FeSCs) have attacted much attention recently following the discovery of the high-transition-temperature superconductivity in LaFeAs(O,F) [2]. FeSCs have the second highest transition temperature, e.g., the recently achieved $T_c \sim 55$ K in $SmFeAsO_{0.85}$ [3]. It was surprising that iron atoms can play a crucial role in high-T_c superconductors. The FeSCs that have received extensive experimental and theoretical studies include ReFeAsO (Re=La or rare earth) (1111-type) [2, 3], AFe_2As_2 (A=Ba, Sr, Ca, etc) (122-type) [4], LiFeAs (Fig.1a) or NaFeAs (111-type) [5], and FeSe (11-type) [6] (Fig.1b). FeSCs are more tunable than CuSCs as one can control transition temperature not only by doping like in CuSC but also by applying pressure on parent stoichiometric compounds.

The common structural properties among these FeSCs is that iron atoms form two-dimensional layers, in which spins on iron atoms could interact with each other via a super-exchange pathway mediated by non-metallic species [7]. This could be naturally modelled by using a two-dimensional Heisenberg model [7]. This feature is also shared by CuSC whereas copper atoms carry spins. However, the superconducting gap structures of FeSCs and CuSCs may be different [13]. However, recently there is intense debate on the existence of magnetism, especially in Li(Na)FeAs [8–12]. These debates are concentrated on the electronic structure of FeSCs near the Fermi surface.

The most important topic in HTSC is electron-pairing mechanism. More generally speaking, what mechanism supports superconductivity to survive at such a high temperature? Bardeen-Cooper-Schrieffer (BCS) theory [14] stated that the electron-pairing mechanism in conventional superconductors is phonon-assisted thanks to the Fermi-liquid behaviour of electrons in metals making the attraction overcome repulsion near the Fermi surface. However, in HTSC it is broadly believed that phonon alone cannot lead to HTSC. Nevertheless, this belief has never been proven correct carefully. Based on this belief, people would rather like to attribute the dominant pairing mechanism to the magnetism induced by the anti-ferromagnetic (AFM) interaction [15]. The co-existence of the first-nearest-neighbour and second-nearest-neighbour AFM exchange interaction in FeSCs leads to a competition between Neel ordering and collinear ordering [4, 16, 17]. Complicated band structure near the Fermi surface and magnetic properties in FeSC and CuSC are crucial for the understanding of the mechanism of HTSC. However, most of the first-principle calculations performed so far are in the level of local density approximation (LDA) and generalized gradient approximation (GGA) and a satisfactory description of the band structure taking into account electron correlation properly is still rare [10, 17–23]. The hybrid functional such as B3LYP [24] and PBE0 [25] can provide a better description for electron correlation and partially eliminates the self-interaction error by mixing exact exchange. For example, the band gap in various compounds can be predicted more accurately by the density functional theory and hybrid functional than those computed by LDA[37].

In this paper I report *ab. initio* calculations for LiFeAs

*Electronic address: w.wu@imperial.ac.uk

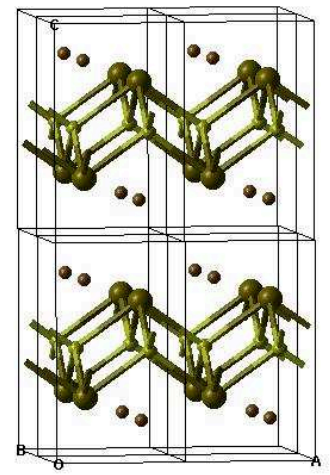

(a)

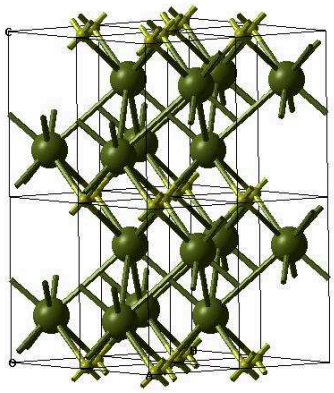

(b)

FIG. 1: (Colour on line.) The structures of a $2a \times 2b \times 2c$ super-cell of LiFeAs (a) and FeSe (b) are shown. In (a) small brown balls are used to label lithium atoms, large brown for arsenic, and small yellow for iron. In (b) large green balls are used to label selenium, and small yellow for iron.

and FeSe by using density functional theory (DFT) and hybrid functional PBE0 [25]. The rest of this paper is organized as the following: in §II I will introduce the computational details, in §III I will show my calculation results and discuss them, and in §IV I will draw some conclusions.

II. COMPUTATIONAL DETAILS

The calculations for electronic structures of LiFeAs and FeSe are carried out by using DFT and hybrid functional PBE0 [25] as implemented in the CRYSTAL 09 code [26]. The basis sets specially designed for lithium[27], iron[28], arsenic[29], selenium[30] atoms in solid-state compounds are used throughout all the calculations. The Monkhorst-Pack samplings [31] of reciprocal space are carried out choosing a grid of shrinking factor to be $8 \times 8 \times 4$ in order to be consistent with the ratios among reciprocal lattice parameters in LiFeAs and FeSe (their experimental tetragonal structures [32, 33] are tabulated in Table I). The truncation of the Coulomb and exchange series in direct space is controlled by setting the Gaussian overlap tolerance criteria to $10^{-6}, 10^{-6}, 10^{-6}, 10^{-6}$, and 10^{-12} [26]. The self-consistent field (SCF) procedure is converged to a tolerance of 10^{-6} a.u. per unit cell (p.u.c). To accelerate convergence of the SCF process, all calculations have been performed adopting a linear mixing of Fock matrices by 30% .

Electronic exchange and correlation are described using the PBE0 hybrid functional [25] which is free of empirical parameters. The advantages of PBE0 include a partial elimination of the self-interaction error and balancing the tendencies to delocalize and localize wavefunctions by mixing a quarter of Fock exchange with that from a generalized gradient approximation (GGA) exchange functional [25].

The broken-symmetry method [34] is used to localize opposite electron spins on each atom in order to describe the AFM state. The exchange couplings in Heisenberg model [35] is defined here as,

$$\hat{H} = J_{1NN} \sum_{ij \in 1NN} \hat{\vec{S}}_i \cdot \hat{\vec{S}}_j + J_{2NN} \sum_{ij \in 2NN} \hat{\vec{S}}_i \cdot \hat{\vec{S}}_j, \quad (1)$$

and determined by

$$J_{1NN} = (E^{1NN}_{\rm FM} - E^{1NN}_{\rm AFM})/(8S^2), \quad (2)$$
$$J_{2NN} = (E^{2NN}_{\rm FM} - E^{2NN}_{\rm AFM})/(4S^2) - 2J_{1NN}. \quad (3)$$

where $E^{1NN}_{\rm AFM}$ and $E^{1NN}_{\rm FM}$ are defined as the total energies of a unit cell, in which the first nearest neighbouring spins are in AFM configuration or ferromagnetic configuration (FM), respectively. J_{1NN} is defined as the first-nearest-neighbouring exchange interaction. The exchange interaction with the second nearest neighbour J_{2NN}, is calculated in a $2a \times b \times c$ super-cell. $E^{2NN}_{\rm FM}$ ($E^{2NN}_{\rm AFM}$) are defined as the total energies with the second-nearest-neighbouring spins aligned (anti-aligned). These formulae are obtained based on the two-dimensional lattice formed by iron atoms as shown in Fig.2.

DFT total-energy calculations have some intrinsic disadvantages for computing exchange interactions, e.g., a comparison between two very large numbers to get a small exchange splitting in an all-electron local basis set formalism. However, the performance of the hybrid functional, e.g., B3LYP or PBE0 as implemented in CRYSTAL has previously been shown to provide an accurate description of the electronic structure and magnetic properties for both inorganic and organic compounds [36–40].

The spin states of iron atoms in LiFeAs and FeSe are still under active debate [8–12]. In this paper, the total energies of the unit cell with non-magnetic, spin-1,

	Symmetry	Lattice constant (Å)	Atomic positions (in fraction)
LiFeAs	P4/nmm (129)	a=b=3.791; c=6.364	Li (0.25, 0.25, 0.8289); Fe (0.75, 0.25, 0.5000); As (0.25, 0.25, 0.2897)
FeSe	P4/nmm (129)	a=b=3.7685;c=5.5194	Fe(0.25, -0.25, 0.0); Se(0.25, 0.25, 0.2877)

TABLE I: The structural parameters for LiFeAs and FeSe.

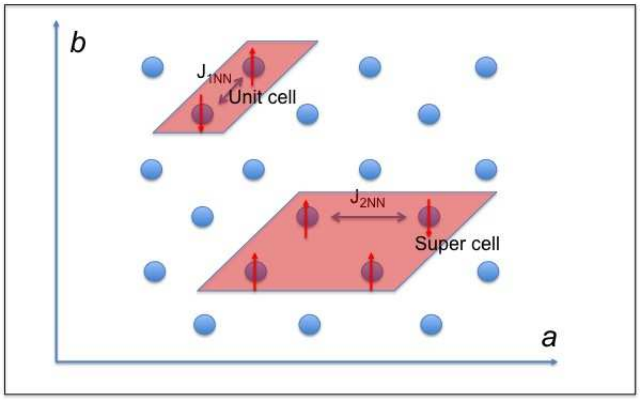

FIG. 2: (Colour on line.) A sketch for the two-dimensional iron layer in LiFeAs and FeSe is shown. Iron atoms are labelled by blue balls. J_{1NN} is the first-nearest neighbour exchange interaction, and J_{2NN} is the second-nearest neighbour exchange interaction. I also show the unit cell and super-cell (doubling the unit cell along lattice vector a) for the computation of J_{1NN} and J_{2NN} respectively. The spin configurations in the unit cell and super-cell as shown here are used to calculate the total energies of AFM configuration $E^{1NN}_{\rm AFM}$ and $E^{2NN}_{\rm AFM}$ respectively.

and spin-2 state for iron atoms are calculated for LiFeAs and FeSe carefully to determine the most stable magnetic state.

III. RESULTS AND DISCUSSIONS

The calculations of a unit cell in LiFeAs and FeSe with 4 unpaired electrons on iron atoms (spin-2 state) are chosen to illustrate the electronic structure and magnetic properties.

A. LiFeAs

I first present the calculation results for electronic structure and magnetic properties of LiFeAs.In total 21 bands are plotted for both AFM and FM configurations. 11 occupied bands are plotted for spin-up and spin-down in AFM configuration. 14(6) occupied bands are plotted for spin-up (spin-down) in FM configuration. The zero energy is chosen to be in the middle of the band gap at Γ point.

In Fig.3 (a), (c), and (e), the band structure, density of states (DOS), and spin densities are presented when the spins on iron atoms in a unit cell are anti-aligned (AFM configuration). The valence band, the conduction band, and another two immediate higher bands for the spin-up and spin-down in AFM configurations and the spin-down in FM configuration are highlighted in red. In the AFM band structure it can be seen that at Γ point there is small gap $\sim$ 1.0 eV between the valence band (VB) and the conduction band (CB). There is also a crossing between VB and CB between Γ and X point. The CB crosses two immediate higher bands as well. These band crossings make AFM configuration look like conducting as shown in DOS (Fig.3c) The largest gap between the VB and CB ($\sim$ 3 eV) can be found at L point.

In Fig.3 (b), (d), and (f), the band structure, density of states (DOS), and spin densities are presented when the spins on iron atoms in a unit cell are aligned (FM configuration). In the FM band structure, there is a rather large gap for spin-up, ranging from $\sim$ 3.5 eV at Γ point to $\sim$ 8.0 eV at L point. By contrast, for spin-down, again we can see there is band crossing around VB and CB. For the spin-down of FM configuration (Fig.3b), the VB crosses CB at X point. And also there are several band degeneracies between Γ and L points. The analysis of the bands near Fermi surface suggests that the hybridization between d-orbitals of iron and $4sp$-orbitals of arsenic atoms is dominant. Again the band crossings make FM DOS look like a half metal; there is clear band gap in the spin-up whereas no gap in spin-down. The Mulliken charge on lithium is $\sim +0.7|e|$, on iron $\sim +0.2|e|$, and arsenic $\sim -0.9|e|$ for AFM and FM configurations. The Mulliken spin densities on irons with spin anti-aligned are $\sim \pm 3.1\mu_B$ for AFM configuration. The discrepancy between this value and the expect one, i.e., $4\mu_B$ may be due to the hybridization between iron and arsenic. For FM configuration, the Mulliken spin densities on irons are $\sim 3.4\mu_B$ and on arsenics are $\sim 0.6\mu_B$. This indicates there is a strong hybridization between iron and arsenic. The Mulliken populations for d-orbitals on the iron atom are also calculated and tabulated in Table.II. The populations of d_{z^2}, d_{yz}, and $d_{x^2-y^2}$ are slightly less than one because the hybridization with $4sp$- orbital on arsenic reduces the populations a bit. The populations of d_{xz} and d_{xy} are almost 0.5 and this implies one unpaired electron may be in a super position between d_{xz} and d_{xy}. The relatively large population of $4sp$-orbitals on arsenic suggests a stronger hybridization in FM configuration.

The projected densities of states (PDOS) of LiFeAs include the projections to the $2sp$-orbitals of lithium atoms (red), the $4sp$-orbitals of iron atoms(green), and d- (blue) and $4sp$ (violet)-orbitals of arsenic atoms. These show that lithium seems to be almost irrelevant and d-orbitals on iron contribute much to the bands near VB and CB.

LiFeAs Mulliken populations								
Orbital	d_{z^2}	d_{xz}	d_{yz}	$d_{x^2-y^2}$	d_{xy}	p_x	p_y	p_z
FM Populations	0.89	0.45	0.70	0.79	0.52	0.23	0.20	0.10
AFM Populations	0.81	0.11	0.74	0.75	0.40	0.02	0.11	0.08

TABLE II: The Mulliken populations for d-orbital of iron atoms and $4sp$-orbital of arsenic atoms are shown.

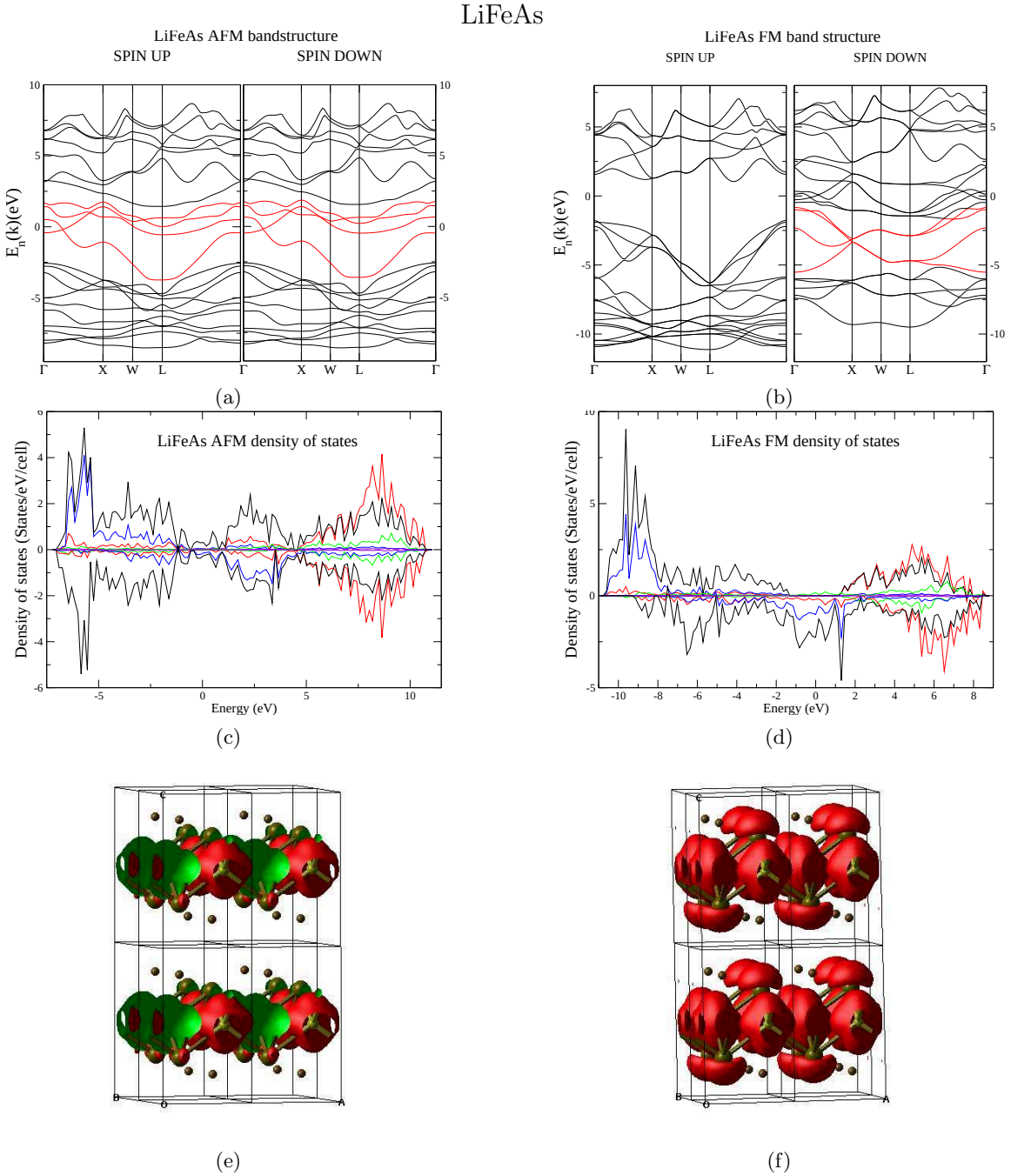

FIG. 3: (Colour on line.) The band structure (a,b), density of states (c,d), and spin densities (e,f) of LiFeAs in AFM and FM configurations respectively are shown. As seen in the electronic structure, AFM configuration looks conducting, whereas FM looks like half-metal because of the band crossing around VB and CB. The projected density of states is multiplied by a factor of 10 to show the orbital contribution, where $2sp$ of lithium is in red, $4sp$ of iron in green, $3d$ of iron in blue, $4sp$ of As in violet, and the total one in black. In spin densities, spin-up is in red, and spin-down in green.

From Fig.3 (e) and (f), it can be seen that the spin densities spread out to arsenic atoms when spins on iron atoms are aligned, and this implies the importance of the hybridization between iron and arsenic. The hybridization to the non-magnetic atoms may be able to shed some new light on the construction of an effective model for the explanation of superconductivity in FeSCs.

The total energies per unit cell for the non-magnetic and spin-1 states are also calculated and both of them are higher than that of the spin-2 state by 6.51 eV and 2.61 eV respectively. So the spin-2 state for iron atom is the most stable state. The exchange interaction in LiFeAs $J_{1\mathrm{NN}}$ is ~ 16 meVs and $J_{2\mathrm{NN}}$ is ~ 81 meVs. The result that $J_{2\mathrm{NN}}$ is larger than $J_{1\mathrm{NN}}$ might be due to different bond angles for the first nearest neighbour and second nearest neighbour. The prediction of an AFM ground state in this work is qualitatively in agreement with recent theoretical results in Ref.[18]. In Ref.[18], it was also concluded that there is an AFM ground state in LiFeAs. However, the details of the band structure in Ref.[18], which largely depends on the functional, are different from the work presented here. The previous work in Ref.[19] suggests that the absence of AFM ordering and points to a triplet pairing mechanism. Based on my results, the system will prefer a collinear ordering because $J_{2NN} > J_{1NN}/2$, i.e., each spin has two ferromagnetically coupling neighbours and another two anti-ferromagnetically coupled ones. Therefore There is some similarity between the work in Ref.[19] and my work. However, my work disagrees with Ref.[22] because they predicted that AFM configuration is higher in energy than non-magnetic one. This might be due to the exclusion of the exact exchange in the functional the authors used in [22]. My work is consistent with the experiments that have shown that there may be strong anti-ferromagnetic fluctuations [11, 12].

B. FeSe

The band structure, DOS, and spin densities for AFM (FM) configuration of FeSe are shown in Fig.4a, c, and e (Fig.4b, d, and f) respectively. In total 21 bands are plotted for both AFM and FM configurations. 11 occupied bands are plotted for spin-up and spin-down in AFM configuration. 14(6) occupied bands are plotted for spin-up (spin-down) in FM configuration. The zero energy is chosen to be in the middle of the band gap at Γ point.

From the band structures of FeSe (Fig.4) we can see that both AFM and FM configurations are insulating although they have different band gap. This is qualitatively different from that in LiFeAs. Once again, the d-orbitals of iron atoms contribute a lot to the bands near the Fermi energy. From the spin densities, it can also been seen that the hybridization between iron and selenium in FM configuration. The Mulliken charge on iron is $\sim +0.3|e|$ and on selenium $\sim -0.3|e|$ for both AFM and FM configurations. The Mulliken spin densities for irons are $\pm 3.6\mu_B$ in the AFM configuration. This value is close to the expected, i.e., $4\mu_B$. For FM configuration, the Mulliken spin densities for irons are $3.7\mu_B$ and for selenium $0.3\mu_B$. This also indicates the hybridization between iron and selenium. The VB and VB-1 for the spin-down in FM configuration are also highlighted in red to illustrate the band degeneracy. The populations of d-orbitals on iron and $4sp$-orbitals on selenium are tabulated in Table.III. The populations of d_{z^2}, d_{xz}, d_{yz}, and $d_{x^2-y^2}$ are slightly less than one suggesting these orbitals are singly occupied although the hybridization reduces the populations a bit. We can also see the hybridization between d-orbitals on iron and $4sp$-orbitals on selenium in FM configuration.

I also compare the total energies per unit cell of FeSe for different spin configurations including spin-0, spin-1, and spin-2. The total energies of spin-0 and spin-1 are higher than that of spin-2 by 5.80 eVs and 1.92 eVs, respectively. This indicates that the spin-2 state is also favoured by FeSe in this tetragonal structure. The exchange interaction in FeSe $\mathrm{J}_{1\mathrm{NN}}$ is approximately 6 meVs and $\mathrm{J}_{2\mathrm{NN}}$ is approximately 13 meVs. This is qualitatively in agreement with the results for FeSe in Ref.[17].

IV. CONCLUSION

DFT calculations combined with hybrid functional PBE0 has been performed for LiFeAs and FeSe tetrahedral structure. The band structures, densities of states, and spin densities are shown and discussed. From these calculations, the AFM configuration of LiFeAs there is band crossing between the valence band and conduction band. By contrast, the AFM configuration of FeSe is insulating. And the FM configuration of LiFeAs show a half-metallic behaviour while FM band structure in FeSe is insulating. The fundamental difference between the band structures of LiFeAs and FeSe might be able to shed some light on the comparison between the experiments on them. As we have seen, the co-existence of localized magnetic moments and the complicated band structure around VB and CB might be the key to answer the question whether LiFeAs is non-magnetic.

The total energies of different spin configurations including non-magnetic, spin-1, spin-2 are also carefully compared for LiFeAs and FeSe, which shows that both of them favour spin-2 state. The exchange interactions of the first nearest and second nearest neighbours are also calculated, and the computed values qualitatively agree with recently experiments and theoretical results leading to a two-dimensional collinear ordering rather than Neel ordering because $J_{2NN} > \frac{J_{1NN}}{2}$. We can also see that from these calculations that the complicated band structures around VB and CB co-exist with collinear ordering induced by the AFM exchange interactions between local magnetic moments on iron atoms.

These calculations are particularly useful for the experimentalists who are concerned with the electron transport, magnetic properties, and electronic structure of the

FeSe Mulliken populations								
Orbital	d_{z2}	d_{xz}	d_{yz}	$d_{x^2-y^2}$	d_{xy}	p_x	p_y	p_z
FM Populations	0.89	0.86	0.86	0.90	0.07	0.10	0.10	0.10
AFM Populations	0.90	0.81	0.82	0.89	0.05	-0.02	0.02	0.0

TABLE III: The Mulliken populations for d-orbital of iron atoms and 4sp-orbital of arsenic atoms are shown.

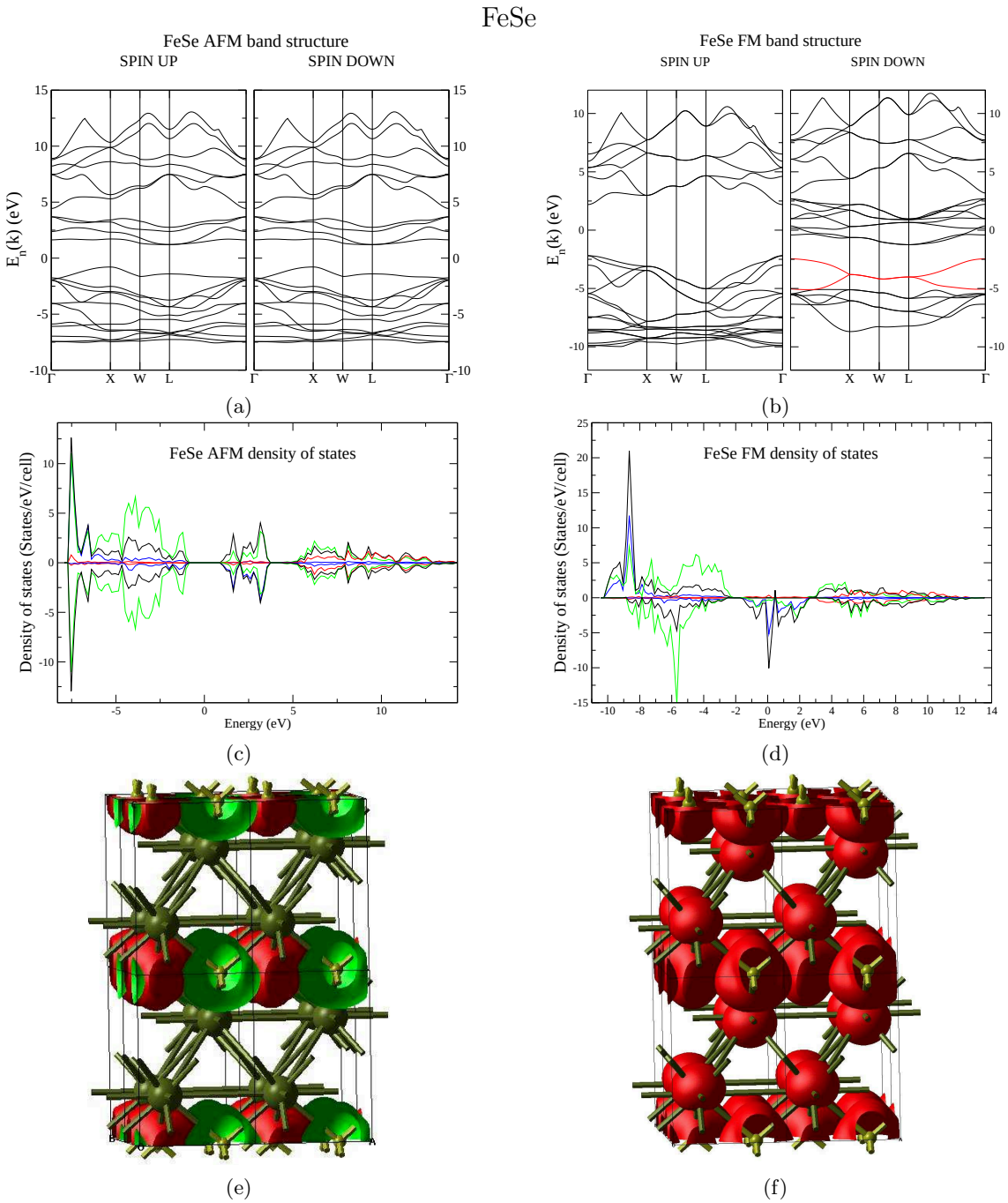

FIG. 4: (Colour on line.) The band structure (a,b), density of states (c,d), and spin densities (e,f) of FeSe AFM (left) and FM (right) configurations respectively are shown. Notice that the band structure suggests that AFM configuration is insulating with a band gap about 2.5 eV by contrast to LiFeAs, whereas FM configuration is half-metal. PDOS are multiplied by a factor of 10 to show the orbital contribution, where 4sp of selenium is in red, 3d of iron in blue, 4sp of iron in green, and the total one in black. In spin densities, spin-up is in red, and spin-down in green.

111-type and 11-type FeSCs. In the future, I would like to build a rather novel effective model based on the electronic structure information provided here to explain superconductivity in FeSCs.

[1] L. Gao, Y. Y. Xue, F. Chen, Q. Xiong, R. L. Meng, D. Ramirez, C. W. Chu, J. H. Eggert and H. K. Mao, Phys. Rev. B, **50**, 4260 (1994).

[2] Y. Kamihara, T. Watanabe, M. Hirano, and H. Hosono, J. Am. Chem. Soc. **130**, 3296 (2008).

[3] Zhi-An Ren, Guang-Can Che, Xiao-Li Dong, Jie Yang, Wei Lu, Wei Yi, Xiao-Li Shen, Zheng-Cai Li, Li-Ling Sun, Fang Zhou and Zhong-Xian Zhao, Europhys. Lett. **83**, 17002 (2008).

[4] M. Rotter, M. Tegel, and D. Johrendt, Phys. Rev. Lett., **101**, 107006 (2008).

[5] J. H. Tapp, Zhongjia Tang, Bing Lv, K. Sasmal, B. Lorenz, P. C. W. Chu, and A. M. Guloy, Phys. Rev. B, **78**, 060505 (2008).

[6] Fong-Chi Hsu, Jiu-Yong Luo, Kuo-Wei Yeh, Ta-Kun Chen, Tzu-Wen Huang, Phillip M. Wu, Yong-Chi Lee, Yi-Lin Huang, Yan-Yi Chu, Der-Chung Yan, and Maw-Kuen Wu, Proc. Nat. Acad. Sci., **105**, 14262 (2008).

[7] E. Abrahams and Qimiao Si, J. Phys. Condens. Matter **23**, 223201 (2011).

[8] S.V. Borisenko,V. B. Zabolotnyy, D.V. Evtushinsky, T. K. Kim, I.V. Morozov, A. N. Yaresko, A. A. Kordyuk, G. Behr, A. Vasiliev, R. Follath, and B. Büchner, Phys. Rev. Lett., **105**, 067002 (2010).

[9] G. F. Chen, W. Z. Hu, J. L. Luo, and N. L. Wang, Phys. Rev. Lett. **102**, 227004 (2009).

[10] C. Platt, R. Thomale, and W. Hanke, Phys. Rev. B, **84**, 235121 (2011).

[11] A. E. Taylor, M. J. Pitcher, R. A. Ewings, T. G. Perring, S. J. Clarke, and A. T. Boothroyd, Phys. Rev. B **83**, 220514(R)(2011).

[12] Meng Wang, X. C. Wang, D. L. Abernathy, L. W. Harriger, H. Q. Luo, Yang Zhao, J. W. Lynn, Q. Q. Liu, C. Q. Jin, Chen Fang, Jiangping Hu, and Pengcheng Dai, Phys. Rev. B **83**, 220515(R) (2011).

[13] T. Y. Chen, Z. Tesanovic, R. H. Liu, X. H. Chen and C. L. Chien, Nature **453**, 1224 (2008).

[14] J. Bardeen, L. N. Cooper, and J. R. Schrieffer, Phys. Rev. **108**, 1175 (1957).

[15] Fa Wang and Dung-Hai Lee, Science, **332**, 200 (2011).

[16] C. de la Cruz, Q. Huang, J. W. Lynn, Jiying Li, W. Ratcliff II, J. L. Zarestky, H. A. Mook, G. F. Chen, J. L. Luo, N. L. Wang and Pengcheng Dai, Nature (London) **453**, 899 (2008).

[17] Fengjie Ma, Wei Ji, Jiangping Hu, Zhong-Yi Lu, and Tao Xiang, Phys. Rev. Lett., **102**, 177003 (2009).

[18] D. J. Singh, Phys. Rev. B **78**, 094511 (2008).

[19] P. M. R. Brydon, Maria Daghofer, Carsten Timm, and Jeroen van den Brink, Phys. Rev. B, **83**, 060501(R) (2011).

[20] A. Subedi, Lijun Zhang, D. J. Singh, and M. H. Du, Phys. Rev. B 78, 134514 (2008).

[21] K. Kusakabe and A. Nakanishi, J. Phys. Soc. Jpn., **78**, 124712 (2008).

[22] Xinxin Zhang, Hui Wang and Yanming Ma, J. Phys.: Condens. Matter **22** 046006 (2010).

[23] L. Hozoi and P. Fulde, Phys. Rev. Lett. **102**, 136405 (2009).

[24] A. D. Becke, J. Chem. Phys. **98**, 5648 (1993).

[25] C. Adamo and V. Barone, J. Chem. Phys., **110**, 6158 (1998)

[26] R. Dovesi, V. R. Saunders, C. Roetti, R. Orlando, C. M. Zicovich-Wilson, F. Pascale, B. Civalleri, K. Doll, N. M. Harrison, I. J. Bush, P. DArco, and M. Llunell, CRYSTAL09 User's Manual (University of Torino, Torino, 2009).

[27] M. Merawa, P. Labeguerie, P. Ugliengo, K. Doll, R. Dovesi, Chem. Phys. Let. **387**, 453-459 (2004).

[28] I. de P.R. Moreira, R. Dovesi, C. Roetti, V.R. Saunders, R. Orlando, Phys. Rev. B **62**, 7816-7823 (2000).

[29] L. A. Curtiss, M. P. McGrath, J-P. Blandeau, N. E. Davis, R. C. Binning, Jr. L. Radom, J. Chem. Phys. **103**, 6104 (1995).

[30] Mike Towler's basis set on CRYSTAL website

[31] H. J. Monkhorst and J. D. Pack, Phys. Rev. B **13**, 5188 (1976).

[32] I. R. Shein and A. L. Ivanovskii, Phys. Rev. B, **78**, 060505 (2009).

[33] Zhaofei Li, J. Ju, J. Tang, K. Sato, M. Watahiki, and K. Tanigaki, J. Phys. Chem. Solid, **71**, 495 (2010).

[34] L. Noodleman, J. Chem. Phys. **74**, 5737 (1980).

[35] W. Heisenberg, Z. Phys. **49**, 619 (1928).

[36] F. Illas, I de P.R. Moreira, C. de Graaf and V. Barone, Theo. Chem. Acc, **104**, 265 (2000).

[37] J. Muscata, A. Wanderb, and N.M. Harrison, Chem. Phys. Lett. **342**, 397 (2001).

[38] S. Heutz, C. Mitra, Wei Wu, A. J. Fisher, A. Kerridge, A.M. Stoneham, A. H. Harker, J. Gardener, H.-H. Tseng, T. S. Jones, C. Renner, and G. Aeppli, Adv. Mat., **19**, 3618 (2007).

[39] W. Wu, A. Kerridge, A. H. Harker, and A. J. Fisher, Phy. Rev. B **77**, 184403 (2008).

[40] W. Wu, A. J. Fisher, and N. M. Harrison, Phys. Rev. B, **84**, 024427 (2011).